Experimental electron-detachment cross sections for collisions of O_2^- with N_2 molecules in the energy range 50–7000 eV

M. Mendes,[1,2] C. Guerra,[1] A. I. Lozano,[1] D. Rojo,[1] J. C. Oller,[3] P. Limão-Vieira,[2] and G. García[1,4,*]

[1]*Instituto de Física Fundamental. Consejo Superior de Investigaciones Científicas, Serrano 113-bis, 28006 Madrid, Spain*

[2]*Atomic and Molecular Collisions Laboratory, CEFITEC, Department of Physics, Universidade NOVA de Lisboa, 2829-516 Caparica, Portugal*

[3]*Centro de Investigaciones Energéticas Medioambientales y Tecnológicas (CIEMAT), Avda. Complutense 22, 28040 Madrid, Spain*

[4]*Centre for Medical Radiation Physics, University of Wollongong, NSW 2522 Australia*

(Received 16 April 2019; published 24 June 2019)

An experimental setup has been implemented to obtain absolute total electron detachment cross sections and relative ionization cross sections in the energy range 50–7000 eV in gas-phase collisions between anionic beams and neutral molecular targets. The primary anionic beam (O_2^-) is produced through a pulsed hollow cathode discharge-induced plasma, deflected and focused towards the collision region where the molecular target is maintained at a well-known pressure. Electron detachment cross sections are measured from the attenuation of the O_2^- beam after interaction with N_2 molecules confined in a gas cell. Negative and positive fragment ions produced during the collisions are extracted and mass analyzed by time-of-flight mass spectrometry. Relative ionization cross sections are derived from the ratio of the measured positive ion fragment intensities (N_2^+, N^+) to the primary O_2^- beam intensity.

DOI: 10.1103/PhysRevA.99.062709

I. INTRODUCTION

Collisions between electrons and atoms and/or molecules have extensively been studied for decades within the scope of different research fields (fundamental and applied). In particular, during the last 20 years, special attention has been paid to their interactions with biomolecules in order to understand the underlying molecular and atomic mechanisms inducing radiation damage [1–5]. Although free electron attachment processes have revealed to be an efficient way to produce such damage [3,4], they may not be sufficiently representative to completely describe the induced molecular fragmentation in biological media. Other electron-transfer processes from neutral projectiles also play relevant roles in a variety of environments, particularly in biomolecular systems [6–11].

There is particular interest in obtaining comprehensive knowledge of ion interactions with atoms and molecules, especially in themes related to astrophysics and interstellar medium, but with increasing interest in biological effects. The production of excited negative and positive ions and free radicals especially those that are oxygen derived, termed reactive oxygen species (ROS), plays a significant role in planetary systems and in biology and medicine [12]. The overproduction of ROS results in oxidative stress in cellular environment destabilizing a cell's integrity, a mechanism that seems to be operative in the case of tumor cells. Additionally, the interaction of radiation with biological matter, in the case of radiation therapy, yields high levels of ROS. In living systems the superoxide anion (O_2^-) is one of the by-products formed by the interaction of free electrons with oxygen molecules, which subsequently interact with other surrounding molecules producing several highly reactive species, like hydrogen peroxide and peroxynitrite, resulting in severe damage for key physiological components [13]. Therefore, accurate cross-section results for these processes are extremely relevant to the use of radiation in medicine and in the development and optimization of new radiotherapy protocols. However, the fundamental description of such molecular induced dissociations and their efficiency to produce biological damage are still poorly known. Another interesting aspect pertains to simple molecules such as O_2, N_2, CO, CO_2, and CH that are important constituents of numerous interstellar environments [14,15]. For instance, it was shown that the superoxide radical ion (O_2^-) can be formed directly on Mars-analog mineral surfaces exposed to ultraviolet radiation under a simulated Martian atmosphere [16].

From a literature survey, we note that several studies have been published regarding collisions between ions and atoms/molecules, with special relevance to ionization cross-section measurements of positive ion projectiles colliding with simple molecules [14,17–21]. However, the studies using negative oxygen ions as projectiles are still fairly scarce, particularly for relatively low-energy collisions (<1000 eV). Some studies on collisions of O_2^- with N_2 reported experimental and theoretical calculations for the total electron detachment cross sections. For high impact energies ($>30\,000$ eV) Jalbert *et al.* [22] showed that the electron detachment cross sections for different incident anions in N_2 present maximum values for projectile velocities around 0.4 a.u. They interpreted this behavior as a shape resonance that also appears in electron-N_2 collisions [22] for equivalent electron incident velocities. These authors have also proposed a semiempirical model to extrapolate cross-section

*Corresponding author: g.garcia@csic.es

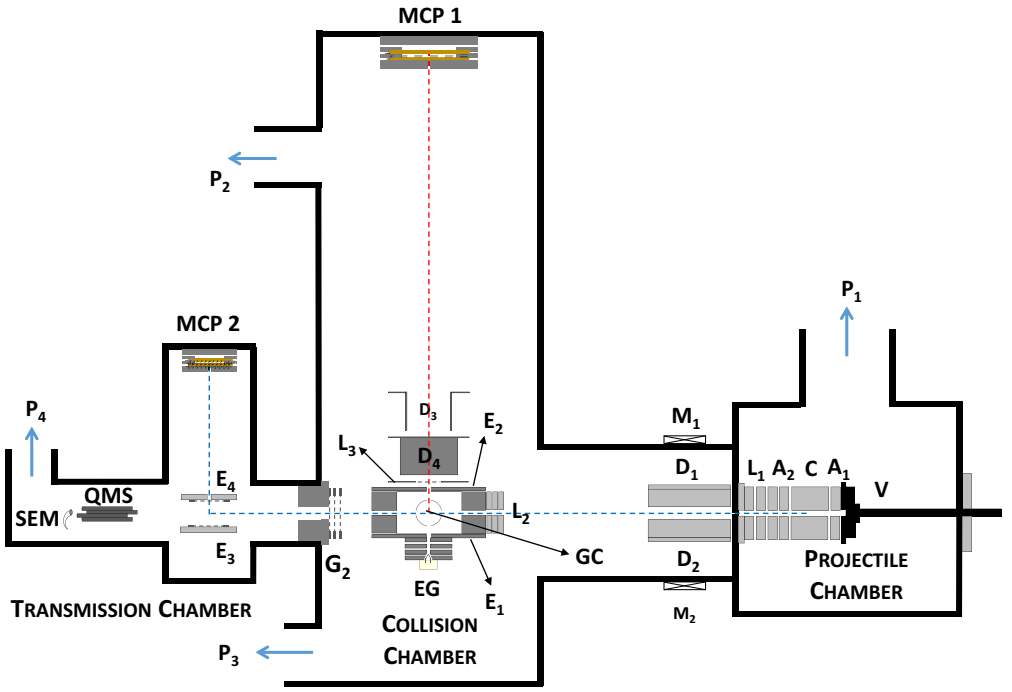

FIG. 1. Schematics of the experimental setup with: V, pulsed supersonic valve; C, hollow cathode discharge; A_1 and A_2, anodes; L_1, L_2, and L_3, Einzel lenses; D_1, D_2, D_3, and D_4, deflecting plates; M_1 and M_2, magnets; E_1, E_2, E_3, and E_4, extraction plates; G_2, focusing/attenuation grids; EG, electron gun; GC, gas cell; MCP 1 and MCP 2, multichannel plate detectors; QMS, quadrupole mass spectrometer; SEM, secondary electron multiplier detector; P_1, P_2, P_3, and P_4, turbomolecular pumps.

values for lower energies. Interesting to note that in $H^- - N_2$ collisions, a similar behavior has been observed [23–25] but is attributed to excitation of the $^2\Pi_g$ resonant state of the nitrogen molecule. Bennett *et al.* [26] have also performed measurements using different incident beams and different targets (including O_2^- in N_2) in the energy range 1–4 keV showing an almost flat energy dependence of the cross section in this range but giving an absolute value in clear disagreement with the aforementioned extrapolation. Above 4 keV, old measurements from Doering [27] and Matić and Čobić [28] showed a cross-section increment (10^{-16}–10^{-15} cm^2) for increasing ion incident energies up to 10–30 keV, although no local maxima were found. Inelastic collisions between atomic anions (H^-, O^-, and Cl^-) and molecules (H_2, O_2, and Cl_2) were also investigated by Hasted and coworkers [29–32], where large cross-section values at low energies have been obtained and interpreted as due to the prevalence of excited states of the negative ions. Finally, O^- and S^- collisions with atoms and molecules were studied by Penent *et al.* [33] and Bomsellek and Esaulov [34,35] giving a detailed analysis of the mechanisms involved in open-shell atom interactions by studying ionizing processes and electron ejected spectra. A previous review of these electron detachment mechanisms for atomic negative ions can be found in Ref. [36].

In this study we report on the absolute total electron-detachment cross sections in the energy range from 50 to 7000 eV as measured with a transmission-beam attenuation technique. In addition, total and partial ionization cross sections have been derived by correlating the observed ionic fragment intensities with the O_2^- beam intensity.

The remainder of this paper is organized as follows: in Sec. II, we briefly introduce and describe the experimental setup used to analyze collisions of oxygen negative ions with nitrogen gas-phase molecules. In Sec. III, we detail the data acquisition methodology and the respective uncertainty sources, while in Sec. IV we present and discuss our electron-detachment cross-section results and the observed total and partial ionization cross sections. The final conclusions are summarized in Sec. V.

II. EXPERIMENTAL SETUP

The experimental setup used in the present study is based on that which has already been reported elsewhere [37] but is described here with some improvements and modifications to the original configuration. It mainly consists of three interconnected high-vacuum chambers (projectile, collision, and transmission chambers) differentially pumped to reach an ultimate base pressure of 3.2×10^{-8} mbar. A schematic diagram of the apparatus is shown in Fig. 1. In the first chamber the oxygen anionic beam is produced through a pulsed hollow cathode discharge that induces oxygen plasma pulses by applying -560 V to the cathode when the anode is grounded (Fig. 2). The negative ions are formed in the afterglow, once the plasma generated species de-excite and secondary electron attachment and charge exchange processes occur. The precursor gas projectile (O_2) was admitted into vacuum through a commercial Parker pulsed valve (VAC1250) operated at 350-μs width in an 80-ms duty cycle and at a gas pressure of 4.0×10^{-5} mbar. The projectile beam is then focused and deflected towards the collision

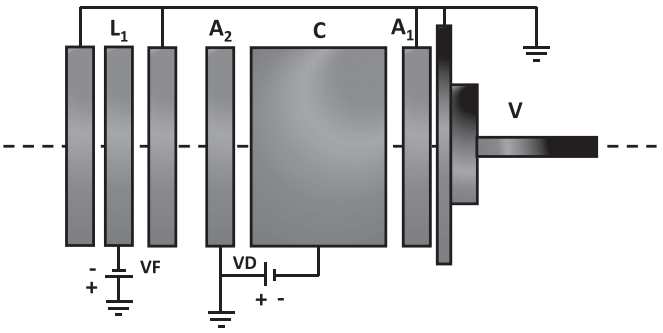

FIG. 2. Electrical schematics of the anion beam source. *V*, pulsed valve; A_1 and A_2, anodes; *C*, hollow cathode; L_1, Einzel lens; VD, discharge voltage; VF, focusing voltage.

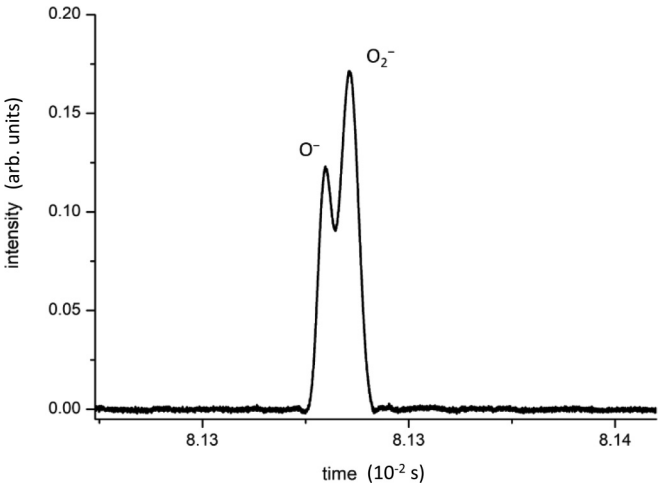

FIG. 3. Time-of-flight mass spectrum of the projectile beam (O_2^-/O^-) at 200 eV in the laboratory frame.

chamber through a combination of an Einzel lens (L_1) placed just after the anode and *XY* deflecting plates (D_1 and D_2) placed at the entrance of the second chamber (Fig. 1). Two magnets are placed outside the chamber in the same region of the deflection plates avoiding stray electrons passing to the collision region. In the second chamber (collision chamber) the anionic projectile beam reaches the gas cell (GC) where the neutral molecular target is maintained at a well-known constant pressure. The GC is a small cylindrical chamber 36 mm in diameter and 27 mm in height, where a negative or positive voltage is applied to accelerate or decelerate the anion beam so defining the kinetic energy of the O_2^- anions and, therefore, the collision energy. The incident anionic beam enters the chamber through a 2-mm diameter hole after being focused by an Einzel lens (L_2) placed just at the entrance of the GC. During all measurements, a negative variable voltage of 210–480 V is applied to the central electrode of L_2 to increase the beam's intensity in the collision region. The molecular target is introduced into the GC through a 15-mm diameter aperture controlled by a leak sapphire valve. During the collision process, positive and negative fragments of the molecule target are formed via ionization and electron transfer processes are able to be alternatively extracted and accelerated in a perpendicular direction to the incident anionic (projectile) beam by means of an extractive plate system. In the present study only positive fragments of nitrogen were recorded since N_2^- autodetachment lifetime is very short lived (a few femtoseconds) [38]. The ion's extraction system is formed by two parallel plates (E_1, E_2) along the GC. A pulsed +950 V between E_1 and E_2 is applied during 2 μs in order to push the resulting cation fragments into a 1.40-m long time-of-flight (TOF) mass spectrometer, where ions are mass analyzed and detected by a microchannel plate (MCP1) operating in single pulse counting mode. Under the gas cell (GC) a homemade electron gun provides an energy controlled electron beam (0–500 eV electron incident kinetic energy) entering the SC perpendicular to the anion beam and opposite to the TOF mass analyzer. The electron gun is not strictly necessary but it is useful to analyze the molecular composition of the background and the gas target as well as to heat the chamber to facilitate its evacuation when needed.

If no voltage is applied to the extractive plate system, the anionic projectile beam reaches the transmission chamber through where it is repelled by – 250 V applied to E_3 towards the second TOF spectrometer where its signal intensity can be monitored by a microchannel plate (MCP2) placed 10 cm just above the plane normal to its initial main direction at 0.47 m from the hollow cathode source (Fig. 1). Before entering this second extraction region, oxygen negative ions pass through a set of three grids (G_2) (the outer two are grounded and the central is connected to a variable voltage ranging from 0 to −560 V). These grids are essentially used to determine the primary beam energy distribution and therefore, the energy resolution of the total cross-section measurements. A typical TOF mass spectrum of the projectile anionic beam is shown in Fig. 3 comprising two main features assigned to O^- and O_2^-

Data acquisition is performed by a high-resolution digital oscilloscope (Tektronix MSO 3034, 2.5 GS/s). Finally, a quadrupole mass spectrometer is placed in the anionic beam optical path (forward direction) to detect any possible neutral fragments that may be produced in the collision between the anionic projectile beam and the gas-phase targets, i.e., O and O_2.

III. DATA ACQUISITION METHODOLOGY

A. Measurement protocol

The total electron detachment cross sections (σ_{exp}) have been obtained through the anionic projectile beam attenuation when the N_2 pressure is varied from 0 to 6 mTorr. The absolute pressure value is determined by means of a MKS Baratron 627B capacitance manometer and a calibrated MKS MicroPirani transducer placed close to the center of the GC but at opposite sites, to detect possible pressure gradients across the GC. The total electron detachment cross-section values (σ_{exp}) were directly derived from the well-known Beer-Lambert law [Eq. (1)]:

$$I = I_0 e - \frac{pl\sigma \exp}{kT}, \tag{1}$$

where *I* is the transmitted anion signal through the gas sample when its pressure is *P*, I_0 is that through the evacuated collision region, *l* is the effective path length of the collision

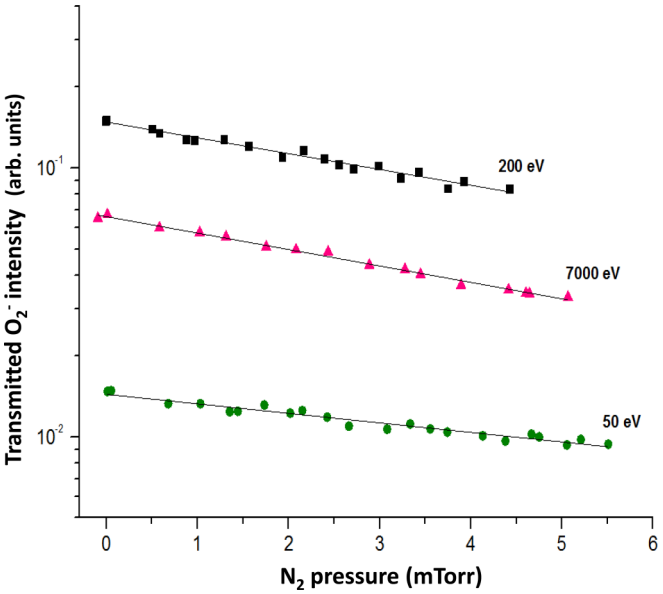

FIG. 4. Typical attenuation signal of O_2^- beam as a function of N_2 pressure in the gas cell for 50, 200, and 7000-eV impact energies.

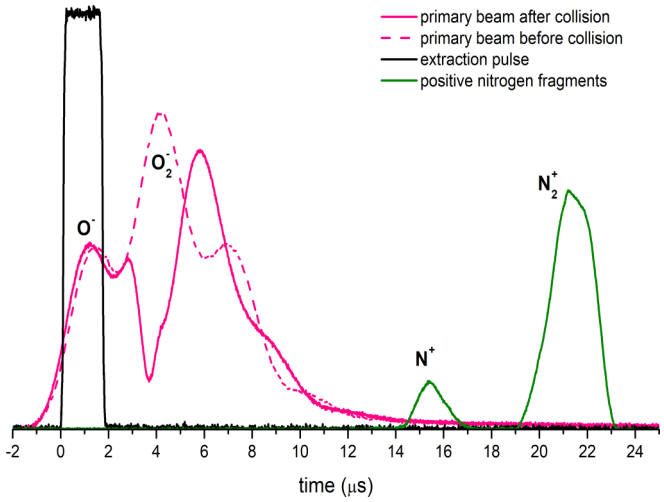

FIG. 5. Typical time-of-flight mass spectrum of N_2 at 560 eV: black line is the extraction pulse at E_1, dashed purple line is the anionic incident beam without N_2 in the gas cell, solid purple line is the transmitted primary beam, and the green line represents the collision resultant positive ions.

region (36 mm), k is the Boltzmann constant, and T is the temperature.

The transmitted intensity is recorded as a function of the gas pressure over an I_0 value, which is reduced to half of its initial value. Figure 4 displays the intensity attenuation signal as a function of pressure for 50, 200, and 7000 eV incident O_2^- beam energy. The slope ($m = l\sigma_{\text{exp}}/kT$) on the semilogarithmic plots provides directly the σ_{exp} values. Note that the straight lines, obtained from least-squares fits to the experimental data, show no systematic deviations so indicating that space charge and multiple scattering effects are negligible for the present experimental conditions.

The partial relative ionization cross sections (σ_+) are obtained through the ratio of the detected positive (N_2^+ and N^+) fragment to the corresponding oxygen (O_2^-) primary beam intensities at the center of the collision chamber for different values of the target gas pressure [Eq. (2)]. For each incident energy, the intensity of the positive ions (I_+) is directly recorded by MCP1, while the O_2^- intensity in the center of the chamber (I_-) is derived from that recorded by MCP2 (transmitted O_2^- intensity) but corrected for the attenuation suffered from the center to the exit of the gas cell. The total relative cross sections are then the sum of the partial cross sections:

$$\sigma_+ = \frac{I_+}{I_-}\frac{1}{nl} \tag{2}$$

A typical TOF mass spectrum of N_2 with O^-/O_2^- is shown in Fig. 5 at an impact energy of 560 eV. At such collision energy several processes may be operative: electron detachment, Eq. (3), electron detachment ionization, Eq. (4), electron detachment dissociative ionization, Eq. (5), and charge exchange to shape resonances (CESR), Eq. (6). The TOF mass spectrum shows only the detection of two cations, N^+ and N_2^+, where the ionization process yielding N_2^+ formation is dominant relative to dissociative ionization yielding N^+:

$$\mathbf{O_2^-} + \mathbf{N_2} \rightarrow \mathbf{O_2} + \mathbf{N_2} + \mathbf{e^-}, \tag{3}$$

$$\rightarrow \mathbf{O_2} + \mathbf{N_2^+} + \mathbf{2e^-}, \tag{4}$$

$$\rightarrow \mathrm{O_2} + \mathrm{N^+} + \mathrm{N} + \mathrm{2e^-}, \tag{5}$$

$$\rightarrow \mathrm{O_2} + \mathrm{N_2^-} \rightarrow \mathrm{O_2} + \mathrm{N_2} + \mathrm{e^-}. \tag{6}$$

Figure 5 also shows the extraction pulse (black line) that is synchronized with the pulsed valve setting the TOF time scale. This can be delayed to select which part of the primary beam (dashed purple line) is effectively generating the observed ionization process. The transmitted O^-/O_2^- anion intensity (solid purple line) is finally detected by MCP2 and therefore is delayed with respect to the extraction pulse (note the path length between the center of the gas cell where the extracting pulsed is applied and MCP2). This timing procedure allows us to select the mass of the primary anion species (O^- or O_2^-) by simple time filtering. Note that the difference between the two purple curves represents the fraction of the selected primary beam, which is generating the positive ions (green line) that have been assigned to N^+ and N_2^+.

B. Uncertainty analysis

At least five attenuation measurements have been performed for each considered energy in order to obtain statistical uncertainties within 5%. Due to the pressure gradient measured along the SC, a correction in pressure was also applied in order to accurately determine its value in the collision region. From the set of measurements a correction factor of 1.15 was applied to σ_{exp}, with an associated uncertainty of $\sim$8% and by adding *in quadrature* all the known error sources and statistical uncertainties, a total uncertainty limit within 7–9% has been determined for the σ_{exp} values.

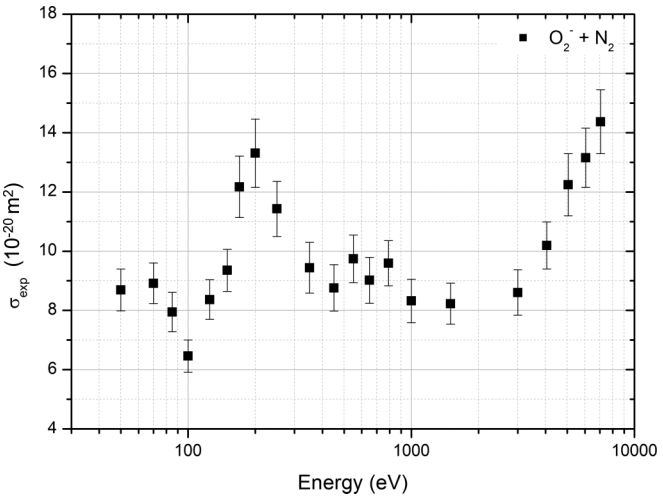

FIG. 6. Electron detachment cross sections in the 50–7000 eV energy range for O_2^- collisions with N_2.

IV. RESULTS AND DISCUSSION

A comprehensive investigation of the electron detachment cross sections (σ_{exp}) has been performed in a wide range of energies, from 50 up to 7000 eV, for collisions of O_2^- with N_2 molecules. The corresponding results are presented in Fig. 6 and the numerical values are also tabulated in Table I.

The experimental cross-section values between 50 and 3000 eV present a minimum at ∼100 eV and a significant enhancement at ∼200 eV (peaking at 13.3×10^{-16} cm^2). Above 3000 eV the cross-section monotonically increases reaching a value of 14.4×10^{-16} cm^2 at 7000 eV. Due to the current maximum energy limitation of our experimental system we are not able to determine the behavior above 7000 eV, i.e., whether the cross section continues to rise, reaches a plateau, or even tends to decrease.

TABLE I. Present experimental results of total electron detachment cross sections for N_2 in collisions with O_2^-.

Energy (eV)	σ_{exp} ($\times 10^{-16}$ cm^2)	Statistical uncertainty (%)
50	8.6	8.09
70	8.9	7.68
85	7.9	8.32
100	6.5	8.46
125	8.4	7.99
150	9.4	7.57
170	12.2	8.51
200	13.3	8.64
250	11.4	8.17
350	9.4	9.10
450	8.8	8.95
550	9.7	8.27
650	9.0	8.58
790	9.6	7.98
1000	8.3	8.81
1500	8.2	8.40
3000	8.6	8.90
4050	10.2	7.83
5050	12.2	8.56
6050	13.2	7.62
7050	14.4	7.52

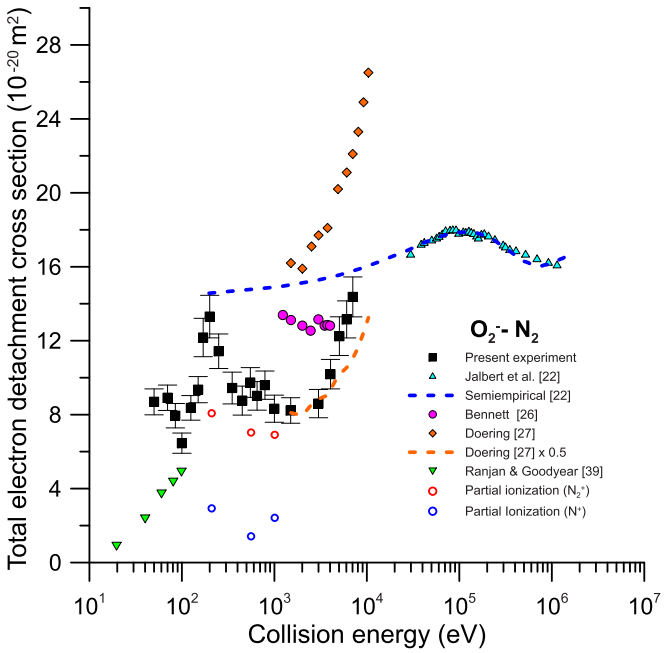

FIG. 7. Total electron detachment cross sections for O_2^- on N_2 (black squares) compared with previously published experimental results from Jalbert *et al.* (blue triangles) and Bennett *et al.* (violet circles), and a theoretical model from Jalbert *et al.* (blue dashed line). The red and blue circles represent the total ionization cross sections for the formation of N_2^+ and N^+, respectively.

As far as we are aware, studies in collisions between negative oxygen ions (O^- and O_2^-) and neutral gas-phase molecules are quite scarce and old, and normally performed at higher energies than those presented in this work. Figure 7 shows the experimental total electron detachment cross sections together with other results available in the literature. Jalbert *et al.* [22] reported total detachment cross sections of O_2^- with N_2 showing a maximum value at 0.4 a.u. (∼130 keV) and decreasing as the energy decreases down to 30 keV (light blue triangles). Additionally, these authors presented a semiempirical use a model to extrapolate their data down to 200 eV (blue dashed line), by assuming that the anion projectile can be viewed as a superposition of a neutral projectile (O_2 core) plus a free electron simultaneously interacting with the molecular target. We should note that this model provides cross-section values with an energy dependence from 200 eV to 7 keV very different from that of the present results, in fact it fails to reproduce the local minimum that we observe at ∼1–3 keV. Older measurements from Bennet *et al.* [26] for incident energies from 1 to 4 keV (see Fig. 7) report absolute values for the total electron detachment cross-section of O_2^- with N_2, which are about 57% higher than the present data at 1 keV but about 13% lower than the semiemprical model from Ref. [22]. The origin of the differences between the results of Bennet *et al.* [26] and Jalbert *et al.* [22] is not clear. Notwithstanding, we believe that the semiempirical model

from Ref. [22] cannot be safely extrapolated to much lower energies, since in the 200–7000 eV incident anion energy range the equivalent (same velocity) electron energy is in the range 0.003–0.12 eV where elastic processes are dominant. We now turn to a close comparison of the present results with the data of Bennett and coworkers [26] within the common energy range, 1–4 keV. Both have similar values for the higher energies, yet their results show cross-section values approximately constant in this energy range thus showing discrepancies with the present data that present a local minimum around 2 keV, where the maximum discrepancy is about 60%. Such a discrepancy has to be attributed to systematic errors existing in the measurement procedures. We note that measurements reported in Ref. [26] were carried out in a continuous beam mode with a relatively high current ($10^{-6}-10^{-7}$ A), so space charge effects may be present in their experimental conditions. In addition they used a Faraday cup detector embedded in the attenuation chamber that may make difficult the determination of the actual absorption length and tend to underestimate the real negative ion current being collected.

Collisional detachment cross sections for O_2^- and O^- on nitrogen were also reported by Doering [27] in the energy range 1.6–10 keV. The results for O_2^- show a similar behavior as the present data. However, in terms of absolute values, Doering's data is about a factor 2 higher than ours. This again seems to be caused by systematic experimental errors. In fact, normalizing these data by a scale factor of 0.5 we obtain cross-section values in good agreement with the present study. Moreover, the results of Ranjan and Goodyear [39] for collisions at incident energies from 20 to 100 eV (see Fig. 7) seem to be compatible with the present data, although with some discrepancies on the behavior of the cross section as a function of the energy. Other results in the impact energy range (15–400 eV) for collisions of O^- with N_2 [40,41] show a similar behavior as the present data for O_2^-, in terms of magnitude, but with no evidence of a local maximum around 200 eV.

Experimental values for collisions of different atomic and molecular anions with different molecular targets in the energy range (5–3600 eV) were analyzed by Hasted and coworkers [30–32]. Although they did not consider the case of O_2^- colliding with N_2, results for analogous processes can be compared with the present measurements in order to look for possible similarities. Detachment cross sections of O^- with N_2 and H^- with H_2 show an increasing tendency up to 400 eV where a plateau is reached, decreasing up to 3600 eV. These authors concluded that direct detachment is the dominant process in these cases, and no negative ions can be formed. However, for O^- with O_2 and O_2^- with O_2 pronounced local maxima are visible around 100 eV followed by an increment of the cross section for higher energies (see Ref. [30]), which behave similarly to the present measurements. Hasted and coworkers associated this behavior with a strong dominance of charge transfer processes, following Massey's assumption [42,43] that a simplified form of "near-adiabatic" theory governs the charge transfer of negative ions. Penent *et al.* [33] found a local maximum around 200 eV (although not so pronounced as that of the present study) for O^- collision with Ar justifying the increment of the cross section to the onset of excitation processes. Some other studies using H^- as incident projectile with N_2 as target, have shown that electron detachment can proceed via formation of a temporary negative ion, in a process known as CESR [24,25,44]. Theoretical and experimental studies based on electron spectroscopy have attributed this to the post-collisional decay of the $N_2^{-2}\Pi_g$ shape resonance formed by charge exchange during the collision.

Another interesting aspect of the collisional process, which may contribute to the observed cross section increment, pertains to the possible role of excited states of the negative ions. In the case of collisions of O^- with rare gas atoms, a maximum around 200 eV has been reported (note that such is also observed in the present data, although with a O_2^- projectile) by Hasted [29] and attributed to excited states of long lifetimes in the negative ion beam. Moreover, an identical rationale was put forward in Cl^- collisions with rare gases (Xe, Ar, He) [29]. Therefore, large cross sections at low energies can also be interpreted as due to the presence of excited states of the ion projectile.

In Fig. 7 we also present the results of N_2^+ and N^+ partial ionization cross sections for three different collision energies (200, 550, and 1000 eV). These are relative values since we cannot give an accurate measure of the absolute beam intensity of the oxygen projectile in the collision region.

At 200 eV the partial relative ionization cross sections for N_2^+ and even more for N^+ production show an increment with respect to those at 500 eV. This may indicate that the maximum of the total electron detachment cross section at 200 eV can partially be associated with ionization processes between O_2^- and N_2, especially those yielding dissociative ionization (i.e., N^+ formation).

Recently, Takahashi *et al.* [45] (and references therein) have reported the relaxation dynamics of doubly excited states as measured with an electron-ion coincidence technique on molecular nitrogen. The generalized oscillator strength distributions of N_2^+ and N^+ showed the mainly autoionizing character of these excited states. It has been commonly accepted that optically allowed doubly excited states of N_2 are observed for photon excitation energies in the 20–40 eV range as broad features [46]. We note that in the photoabsorption spectrum of Codling [47] a discrete structure at 23 eV was assigned to doubly excited Rydberg states $(1\pi_u)^{-1}(3\sigma_g)^{-1}(1\pi_g)^1(ns\sigma_u)^1$ with principal quantum number $n = 4$, 5 converging to the $C^2\Sigma_u^+$ state of N_2^+. Additionally, fluorescence data extended those Rydberg states for $n = 3-10$ and dissociative doubly excited states correlating with satellites of N_2^+ as broad peaks in the range 23–33 eV were reported by Ukai and coworkers [48]. In addition, at 200-eV ion impact energy an average of 10% energy loss to the target may be expected [49] and so, we suggest that the enhancement feature at 200 eV (Fig. 6) is probably due to the role of such double excited states, which by their nature result in either autoionization or neutral dissociation [45]. Such an assumption seems reasonable since we note in Fig. 7 an increment of the N_2^+ and N^+ yields at 200 eV with respect to those at 550 and 1000 eV.

V. CONCLUSIONS

An experimental setup for investigating collisions between anionic beams and neutral gas-phase molecular targets has been described. The anionic beam projectile is produced in

a hollow cathode discharge-induced plasma, guided to the interaction region by a set of focusing electrodes and deflecting plates and made to interact with a neutral molecular target maintained at a constant pressure in the interaction region. With this configuration, it was possible to measure absolute total electron-detachment cross sections for molecular oxygen anions impinging on nitrogen molecules at incident energies ranging from 50 to 7000 eV. Positive TOF mass spectra for N_2 were obtained and relative partial and total ionization cross sections for selected incident energies were also obtained.

The total cross-section measurements have an increasing behavior with energy, showing a local maximum at 200 eV (lab frame). Since no measurements of this type covering the entire energy range were reported previously, to our knowledge, some tentative assignments have been put forward here. Other studies [22,26–30] using different projectile anionic beams (O_2^-, O^-, H^-) and different target molecules have found local maxima in the energy dependence of the electron detachment cross section that may be related to that reported here. The structure at 200 eV was interpreted in the light of different processes either through the decay of a temporary negative ion of $N_2^{-2}\Pi_g$ shape resonance formed by charge exchange [24,25,44], reactions involving excited states of O_2^- or the excitation of doubly excited states leading to ionization. Relative ionization cross sections were also reported for N^+ and N_2^+ and the energy behavior related to N^+ formation (dissociative ionization) is discussed on the basis of double excited states of molecular nitrogen [45–48].

Future improvements and comprehensive work to explore the mechanisms governing anion-molecule collisions, especially through energy loss experiments are mandatory to help in the interpretation of the interaction processes involved in these types of collisions as well as further theoretical contributions to improve our knowledge on such relevant processes.

ACKNOWLEDGMENTS

M.M. and P.L.-V. acknowledge the Portuguese National Funding Agency FCT-MCTES through Grants No. PD/BD/106038/2015, No. UID/FIS/00068/2019, and No. PTDC/FIS-AQM/31281/2017. This work was also supported by Radiation Biology and Biophysics Doctoral Training Programme (RaBBiT, PD/00193/2012); UID/Multi/ 04378/2013 (UCIBIO). G.G. acknowledges partial financial support from the Spanish Ministerio de Ciencia, Innovación y Universidades (Project No. FIS2016-80440).

[1] B. Van Zyl and T. M. Stephen, Phys. Rev. A **50**, 3164, (1994).
[2] V. S. Prabhudesai, A. H. Kelkar, D. Nandi, and E. Krishnakumar, Phys. Rev. Lett. **95**, 143202 (2005).
[3] S. Denifl, P. Sulzer, D. Huber, F. Zappa, M. Probst, T. D. Märk, P. Scheier, N. Injan, J. Limtrakul, R. Abouaf, and H. Dunet, Angew. Chem. Int. Ed. **46**, 5238 (2007).
[4] B. Boudaïffa, P. Cloutier, D. Hunting, M. A. Huels, and L. Sanche, Science **287**, 1658 (2000).
[5] T. Tabata, T. Shirai, M. Sataka, and H. Kubo, At. Data Nucl. Data Tables **92**, 375 (2006).
[6] D. Almeida, R. Antunes, G. Martins, S. Eden, F. Ferreira da Silva, Y. Nunes, G. Garcia, and P. Limão-Vieira, Phys. Chem. Chem. Phys. **13**, 15657 (2011).
[7] P. Limão-Vieira, A. M. C. Moutinho, and J. Los, J. Chem. Phys. **124**, 054306 (2006).
[8] D. Almeida, M.-C. Bacchus-Montabonel, F. Ferreira da Silva, G. Garcia, and P. Limão-Vieira, J. Phys. Chem. A **118**, 6547 (2014).
[9] D. Almeida, F. Ferreira Da Silva, S. Eden, G. García, and P. Limão-Vieira, J. Phys. Chem. A **118**, 690 (2014).
[10] F. Ferreira da Silva, D. Almeida, R. Antunes, G. Martins, Y. Nunes, S. Eden, G. Garcia, and P. Limão-Vieira, Phys. Chem. Chem. Phys. **13**, 21621 (2011).
[11] D. Almeida, R. Antunes, G. Martins, G. Garcia, R. W. McCullough, S. Eden, and P. Limão-Vieira, Int. J. Mass Spectrom. **311**, 7 (2012).
[12] C. von Sonntag, The Superoxide Radical, in *Free-Radical-Induced DNA Damage and Its Repair*, edited by D. S. Schreck (Springer, Berlin, 2006), pp. 159–194.
[13] J. N. Moloney and T. G. Cotter, Semin. Cell Dev. Biol. **80**, 50 (2018).
[14] J. López-Patiño, B. E. Fuentes, F. B. Yousif, and H. Martínez, Int. J. Mass Spectrom. **405**, 59 (2016).
[15] D. T. Hall, D. F. Strobel, P. D. Feldman, M. A. McGrath, and H. A. Weaver, Nature (London) **373**, 677 (1995).
[16] A. S. Yen, S. S. Kim, M. H. Hecht, M. S. Frant, and B. Murray, Science **289**, 1909 (2000).
[17] S. L. Lin, J. N. Bardsley, and D. L. Albritton, Int. J. Mass Spectrom. Ion Phys. **34**, 113 (1980).
[18] H. Kheyrandish, D. G. Armour, and E. J. Jones, Vacuum **34**, 269 (1984).
[19] J. J. Leventhal and L. Friedman, Chem. Phys. **46**, 997 (1967).
[20] F. B. Alarcón, B. E. Fuentes, H. Martínez, and F. B. Yousif, Nucl. Instrum. Methods B **332**, 317 (2014).
[21] W. J. Lichtenberg, K. Bethge, and H. Schmidt-Böcking, J. Phys. B **13**, 343 (1980).
[22] G. Jalbert, R. F. Nascimento, C. R. De Carvalho, C. R. Carvalho, B. F. Magnani, A. C. F. Santos, A. B. Rocha, M. M. S. Anna, and N. V. D. C. Faria, Phys. Rev. A **89**, 012712 (2014).
[23] J. S. Risley and R. Geballe, Phys. Rev. A **9**, 2485 (1974).
[24] V. N. Tuan, V. Esaulov, J. P. Gauyacq, and A. Herzenberg, J. Phys. B **18**, 721 (1985).
[25] V. N. Tuan and V. A. Esaulov, J. Phys. B **15**, L95 (1982).
[26] R. A. Bennett, J. Chem. Phys. **62**, 2223 (1975).
[27] J. P. Doering, J. Chem. Phys. **41**, 1164 (1964).
[28] M. Matic and B. Cobic, J. Phys. B **4**, 111 (1971).
[29] J. B. Hasted, Proc. R. Soc. A **212**, 235 (1952).
[30] J. B. Hasted and R. A. Smith, Proc. R. Soc. A **235**, 349 (1956).
[31] J. B. Hasted and D. Phil, Proc. R. Soc. A **222**, 74 (1954).
[32] J. B. H. Stedeford and J. B. Hasted, Proc. R. Soc. A **227**, 466 (1955).
[33] F. Penent, J. P. Grouard, R. I. Hall, J. L. Montmagnon, R. L. Champion, L. D. Doverspile, and V. A. Esaulov, J. Phys. B **20**, 6065 (1987).
[34] S. Boumsellek and V. A. Esaulov, J. Phys. B **23**, L605 (1990).
[35] S. Boumsellek and V. A. Esaulov, J. Phys. B **23**, 1303 (1990).

[36] V. A. Esaulov, Ann. Phys. Fr. **11**, 493 (1986).
[37] J. C. Oller, L. Ellis-Gibbings, F. F. da Silva, P. Limão-Vieira, and G. García, EPJ Tech. Instrum. **2**, 13 (2015).
[38] G. J. Schulz, Rev. Mod. Phys. **45**, 423 (1973).
[39] R. Ranjan and C. C. Goodyear, J. Phys. B **6**, 1070 (1973).
[40] R. N. Compton and T. L. Bailey, J. Chem. Phys. **53**, 454 (1970).
[41] A. E. Roche and C. C. Goodyear, J. Phys. B **2**, 191 (1969).
[42] *Advances in Atomic Molecular Physics*, edited by H. S. W. Massey, D. R. Bates, and B. Bederson, (Academic, New York, 1979), pp. 1–36.
[43] H. S. W. Massey, Rep. Prog. Phys. **12**, 248 (1949).
[44] J. S. Risley, Phys. Rev. A **16**, 2346 (1977).
[45] K. Takahashi, T. Hasegawa, and Y. Sakai, Eur. Phys. J. D **71**, 1 (2017).
[46] P. Erman, A. Karawajczyk, U. Köble, E. Rachlew, K. Y. Franzén, and L. Veseth, Phys. Rev. Lett. **76**, 4136 (1996).
[47] K. Codling, Astrophys. J. **143**, 552 (1966).
[48] M. Ukai, K. Kameta, N. Kouchi, Y. Hatano, and K. Tanaka, Phys. Rev. A **46**, 7019 (1992).
[49] M. Mendes, B. Pamplona, S. Kumar, F. Ferreira da Silva, A. Aguilar, G. García, M.-C. Bacchus-Montabonel, and P. Limão-Vieira, Front. Chem. **7**, 264 (2019).